Lab 4-Binary Classifier
Stat 215A, Fall 2014

Xiang (Lisha) Li, Jonathan Fischer, Andrew Do, Hye Soo Choi

November 10, 2014

1 Introduction

Blah blah...

2 EDA

2.1 Plots of Raw and Expertly Labelled Images

Figure 1 displays the unprocessed image files for comparison with Figure 2, the expertly-labelled files. With the human eye it is not so difficult to parse cloud from ground based on these images, but we see that cloudy and clear pixels alike run through wide spans of AN so other features must be used.

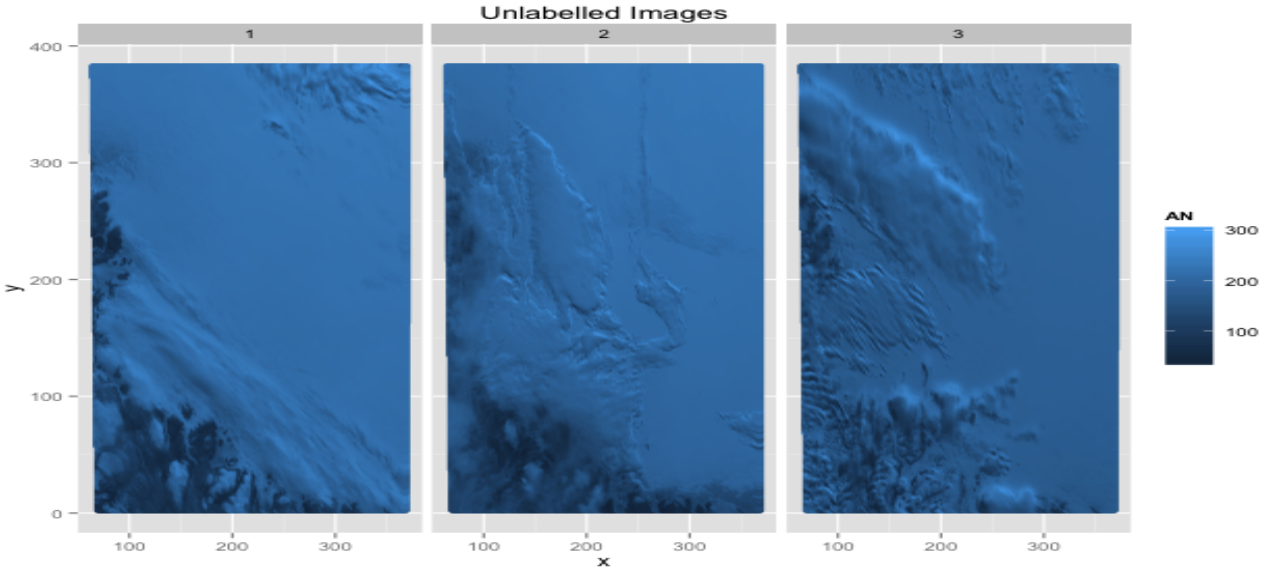

Figure 1: Raw images with AN radiances.

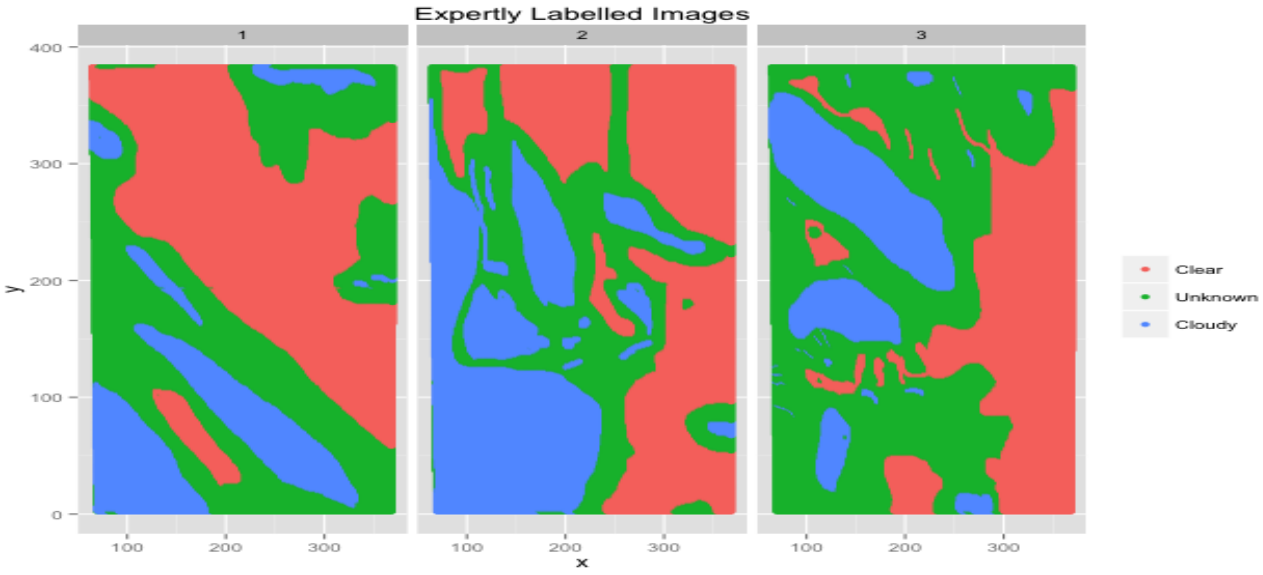

Figure 2: Images with expert classifications. Proportions: 39.8% unknown, 23.4% cloudy, 36.8% clear.

2.2 Densities of NDAI, SD and CORR

The following three plots gives us a sense of what can be learned from NDAI, SD and CORR. The densities are grouped by their expert labels, red is for 'no cloud', green are for 'unknown' and blue for 'cloud'. We can see that NDAI has reasonably good separation between cloud and no cloud, in all three pictures, which is confirmed in our later modeling sections by Gini importance measures found in the random forest model and it's importance as a variable in LDA/QDA and logit models. In comparison, SD does not have as good of a separation within the smaller SD values, however it is still clear that pixels labelled as clouds are the only pixels with higher SD values. We thus expect the two features in combination can help determine whether a pixel with high NDAI should be labelled as a cloud by using the SD feature. Finally CORR values appear to be a good separator for image 2, but much less so for image 1. This uneven distribution of CORR values between images prompted us to cross validate our models across images, in addition to the folds created by dividing each image into 4 quadrants.

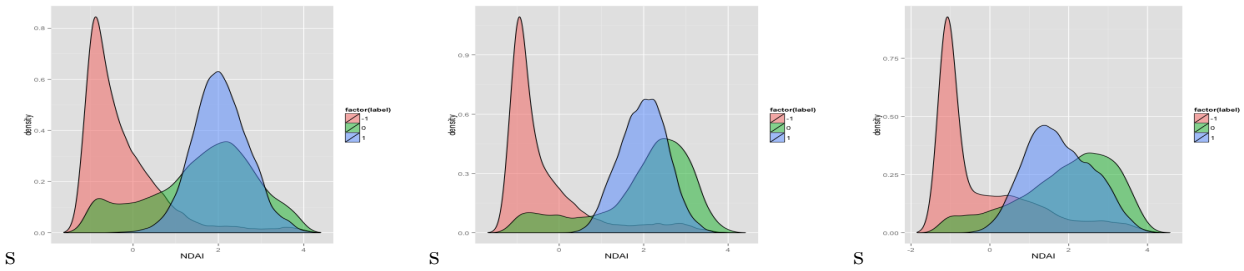

Figure 3: NDAI density plot for Image 1, 2, 3 (respectively).

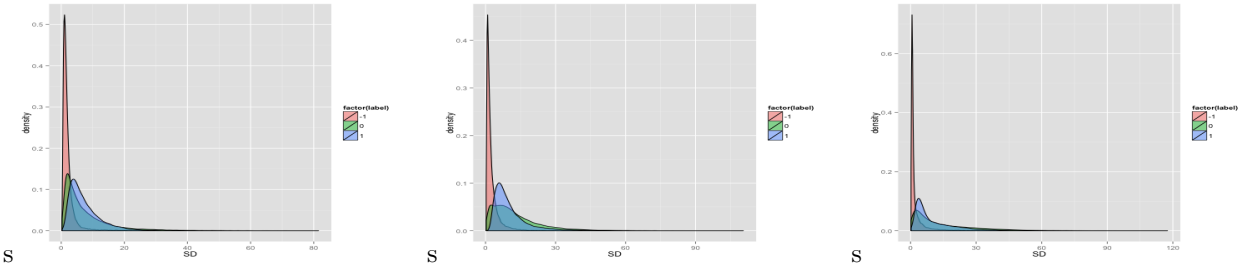

Figure 4: SD density plot for Image 1, 2, 3 (respectively).

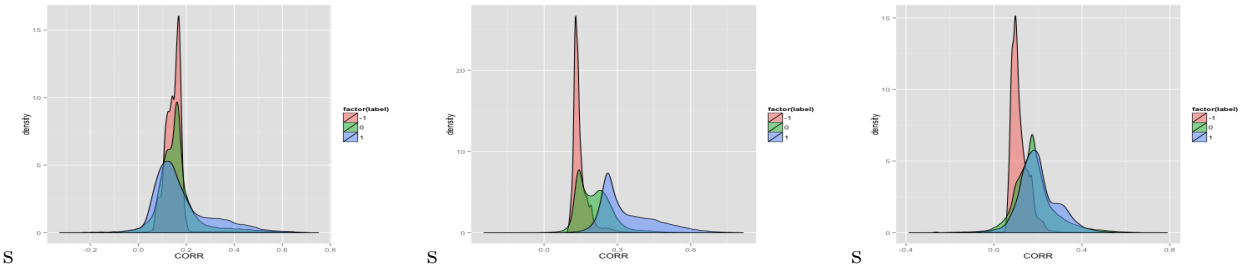

Figure 5: CORR density plot for Image 1, 2, 3 (respectively).

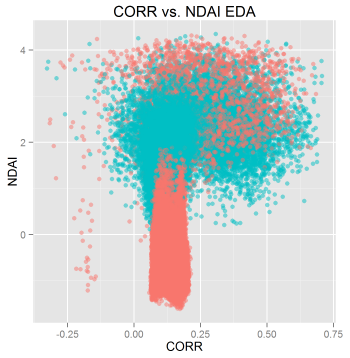

(a) CORR vs. NDAI Plot of Image 1

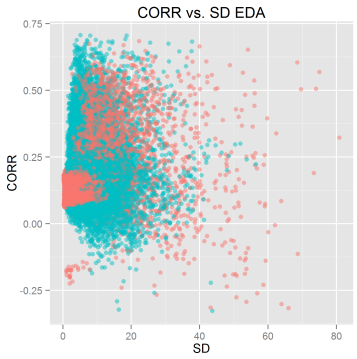

(b) CORR vs. SD Plot of Image 1

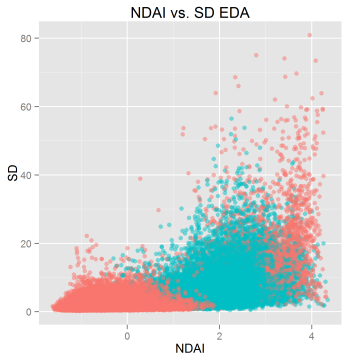

(c) NDAI vs. SD Plot of Image1

Figure 6: Scatter plots of the pairs of features used in the analyses. Red points denote pixels that were labeled as not clouds and blue points represent cloudy pixels.

Figure 6 shows hope that our selected features may be able to distinguish between cloudy and icy pixels. The rounded boundaries suggest that non-linear surfaces may be necessary to separate the feature space.

2.3 Mapped Features

The ensuing figures plot the engineered feature values (NDAI, SD, CORR) spatially. In agreement with the NDAI density plots, higher NDAI values indicate increased likelihood of the presence of clouds, and the NDAI plots look quite similar to the binary classification plots. The SD maps show areas of high variance in the radiances thereby providing a decent outline of cloud boundaries. Unfortunately, this can also lead to the highlighting of uneven ground regions. Finally, the CORR images resemble weakened versions of their NDAI counterparts though with some additional strange behavior in the bottom left corners of Images 1 and 2.

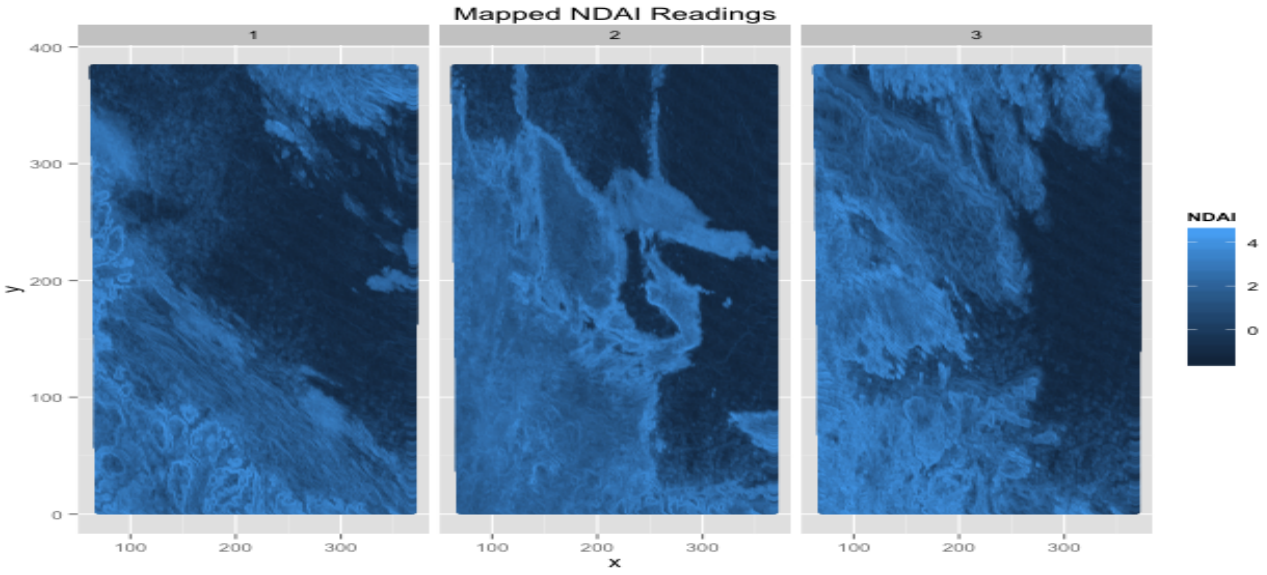

Figure 7: Mapped NDAI readings. We see good correspondence between larger values and presence of clouds.

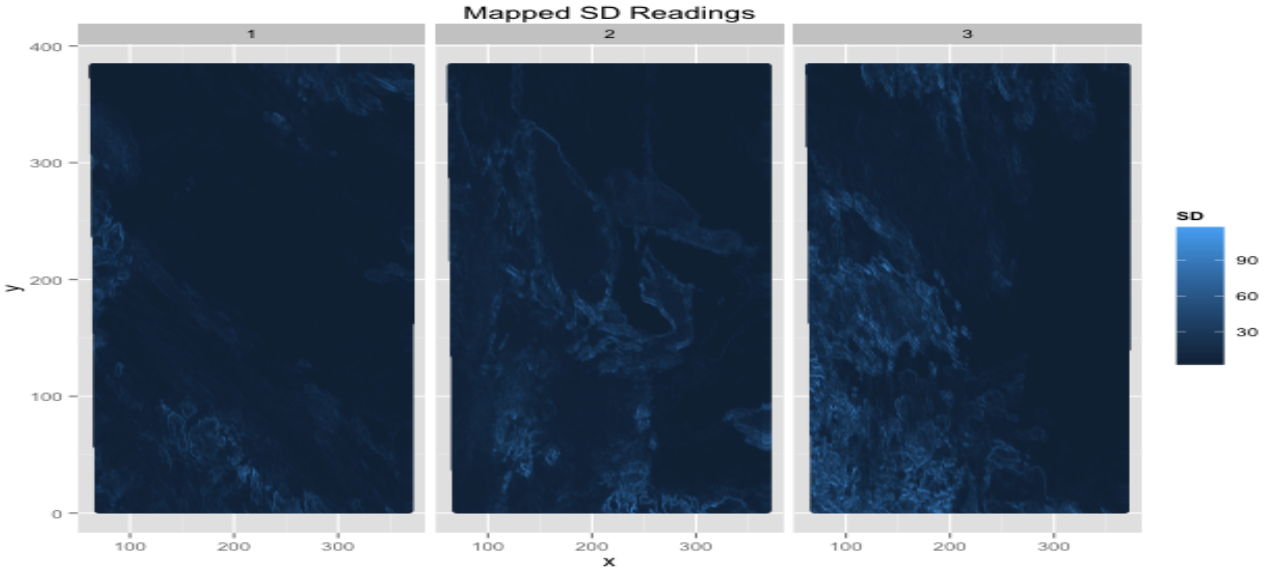

Figure 8: Mapped SD readings. Higher values show cloud boundaries, though also show uneven terrain.

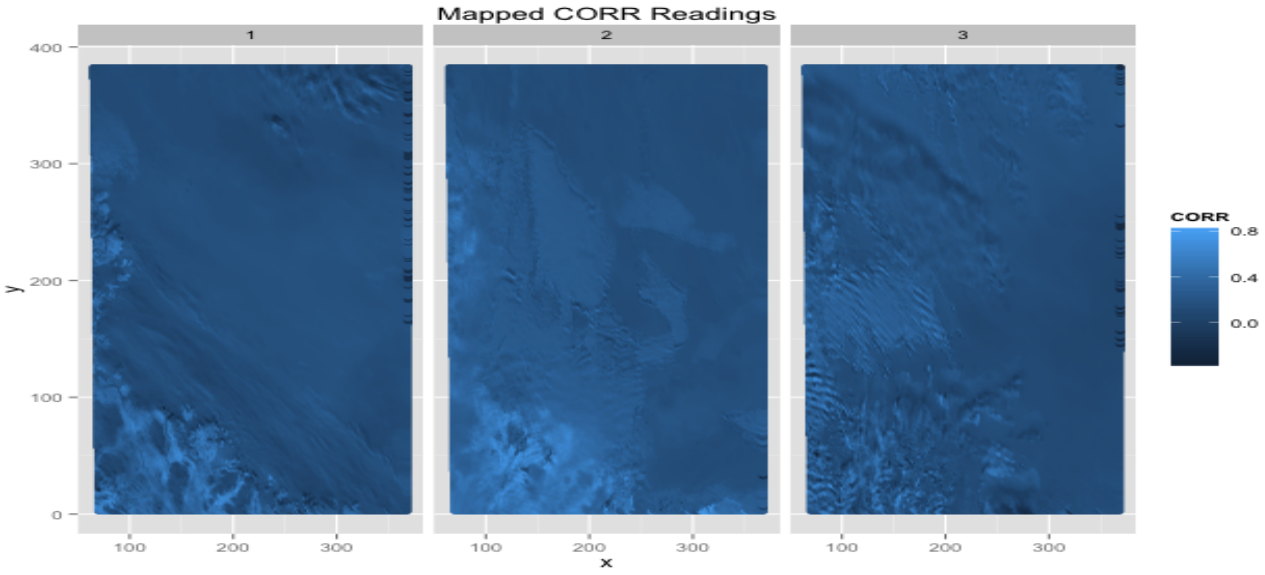

Figure 9: Mapped CORR readings. Cloudy regions tend to be lighter, but not as strongly as in NDAI.

3 Modeling

3.1 QDA/LDA

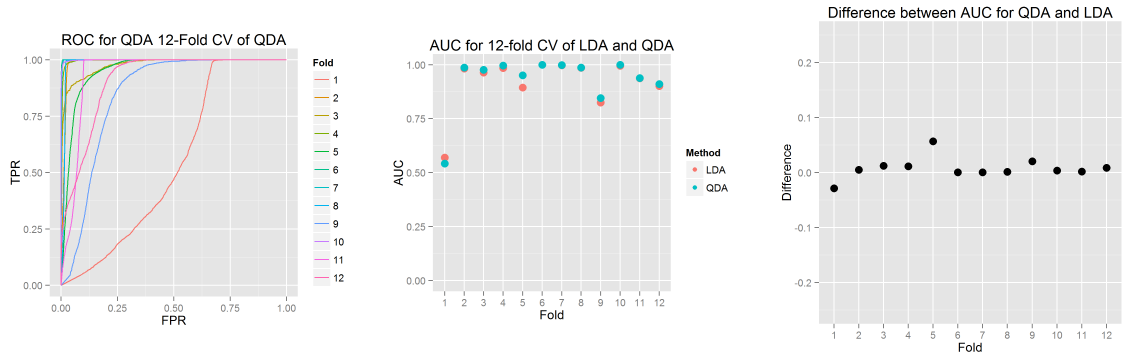

(a) ROC for 12-fold CV of QDA (b) AUC for LDA QDA Classifiers (c) AUC Differences

Figure 10: (10a) shows the ROC curves for each of the 12 folds of cross validation. (10b) and (10c) show evidence via AUC estimates that QDA performs slightly better than LDA. Note that in both analysis, fold 1 has an abnormally low AUC.

Linear discriminant analysis (LDA) for binary classification aims to separate the feature space using a hyperplane. It assumes that the each class is normally distributed with means μ_0 and μ_1 and that the two classes are homoscedastic with covariance matrix $\Sigma_0 = \Sigma_1 = \Sigma$. Quadratic discriminant analysis works in the same manner except that it makes no assumptions about the covariance matrix. Thus given the multivariate Guassian distribution:

$$f_c(x) = \frac{1}{(2\pi)^{p/2}|\Sigma_c|^{1/2}} e^{-\frac{1}{2}(x-\mu_c)^T \Sigma_c^{-1}(x-\mu_c)} \tag{1}$$

where $c = 1, 2$ is the class label. Let p_c be the prior probability of class c. We can calculate the probability

for a case x belonging to class c by:

$$P(x \in \text{ Class } c|X = x) = \frac{f_c(x)p_c}{f_1(x)p_1 + f_2(x)p_2} \tag{2}$$

We can then classify each point by selecting a probability threshold and hard-assigning based on whether or not the posterior probability was higher or lower than that threshold. Both LDA and QDA were carried out during our analyis of the data, but as we suspected from our exploratory data anaylsis, QDA performed slightly better than LDA when we compared the results side-by-side (see figure 10). During cross-validation, each image was divided into four horizontal strips, resulting in 12 folds to be used in our validation procedure. In each iteration, we withheld one of the strips and trained on the remaining 11. The resulting images after piecing the horizontal strips back together can be seen in figure 12. Cross-validation for QDA revealed that while the method works extremely well in some cases, producing AUC scores of almost 1, it sometimes fails to perform better than even the theoretical random classifier. In particular, the classifier does not seem to be good at discerning snow from clouds in regions where there are many dark pixels corresponding to geographical features. The most indicative example of this is seen in image 1 where the algorithm misclassifies an entire ridge-filled region as clouds. We also noticed that there were some misclassifications within large cloudy regions. Figure 11 shows this nicely.

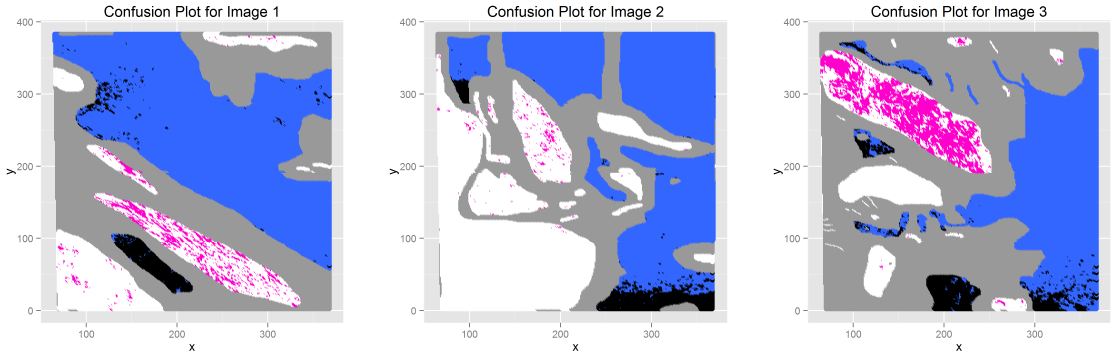

Figure 11: A comparison between the output of QDA and expert labels.

Figure 12: Posterior probabilities of being a cloud as given by QDA

3.2 Logit/Probit

The logit model obtained via averaging after 12-fold cross-validation has $y_i = -3.356 + 1.900 * NDAI_i - 0.074 * SD_i + 9.002 * CORR_i$ where $P_i(\text{Cloud}) = \frac{1}{1+e^{-y_i}}$.

To choose our cutoff value for declaring a pixel cloudy, we varied the cutoffs from .01 to 1 and calculated the misclassification error of our model at that threshold on expertly-labelled pixels. The figure below shows that the optimal threshold for this model is at .38, with an error of just under 10.1%. As a consequence of this low threshold, we observe more false positives than false negatives. This will be further explored below.

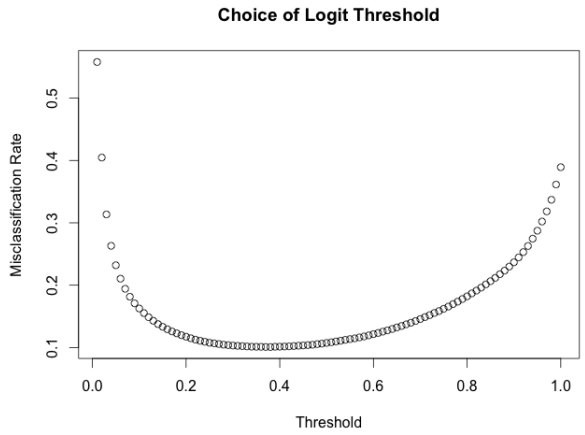

Figure 13: We see a minimum in misclassification rate at .38.

Figure 15 gives the binary classifications overlaid on the images. Visual comparision with the expertly-labelled images suggests that we are slightly biased towards the presence of clouds as 74.2% of unlabelled points have been classified as cloudy, though this may be due to some artifact of the expert labelling scheme.

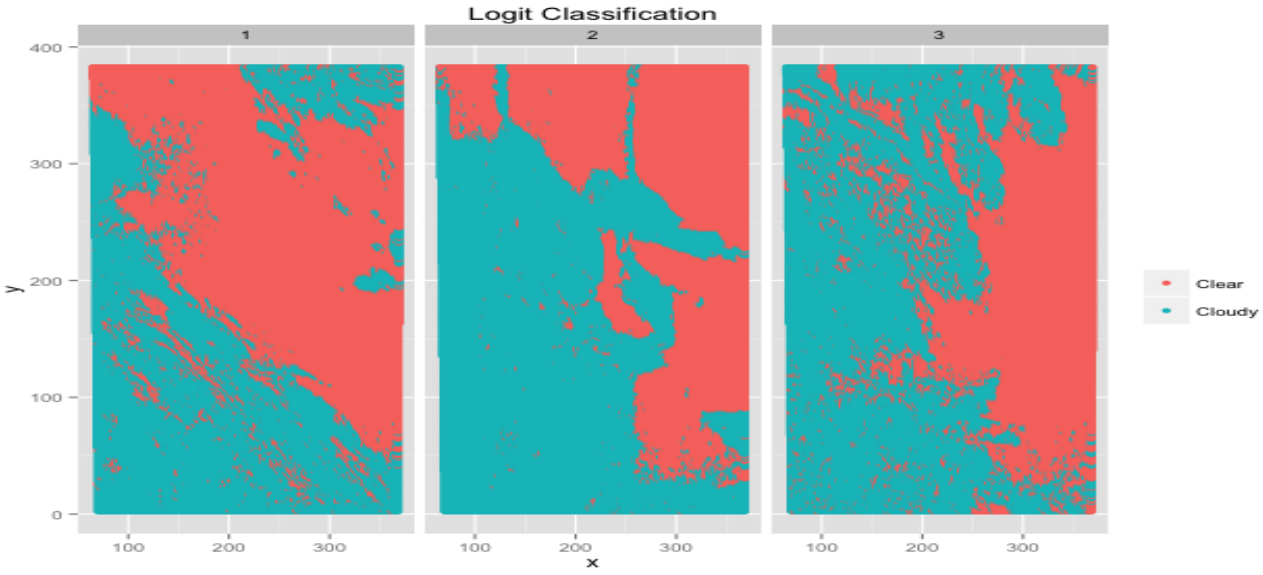

Figure 14: Binary classifications with threshold = .38 for logit trained via 12-fold CV.

Here we see the logit probabilites plotted spatially. This should approximate how the image would appear if the ground were not covered in snow and ice, so comparison with Figure 1 is especially appropriate.

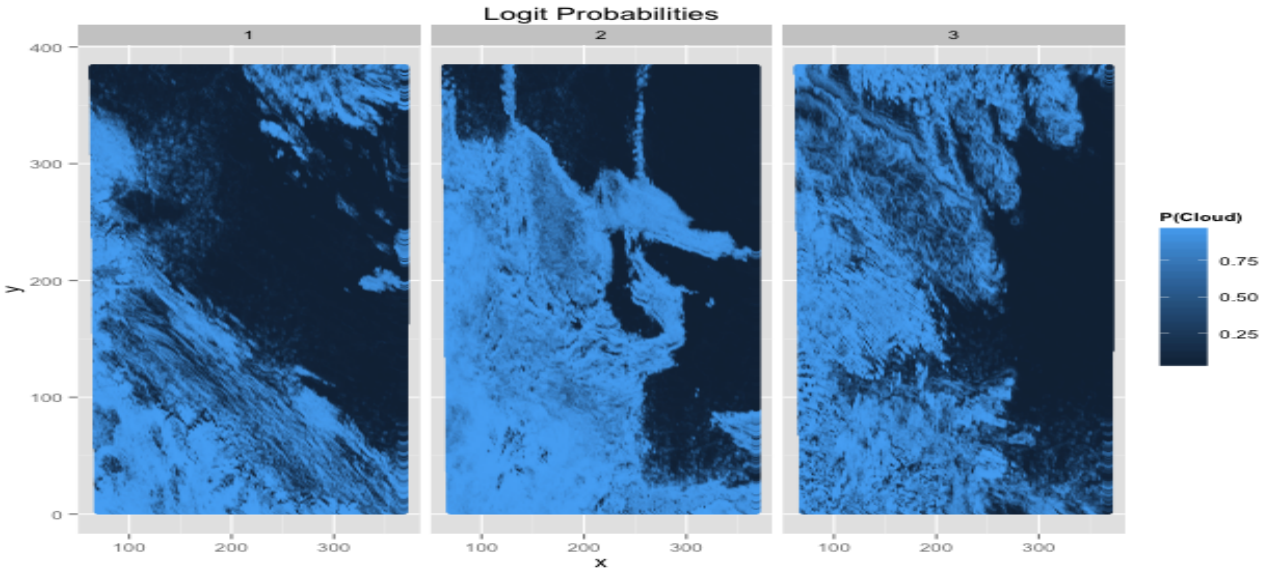

Figure 15: Probabilities for logit trained via 12-fold CV.

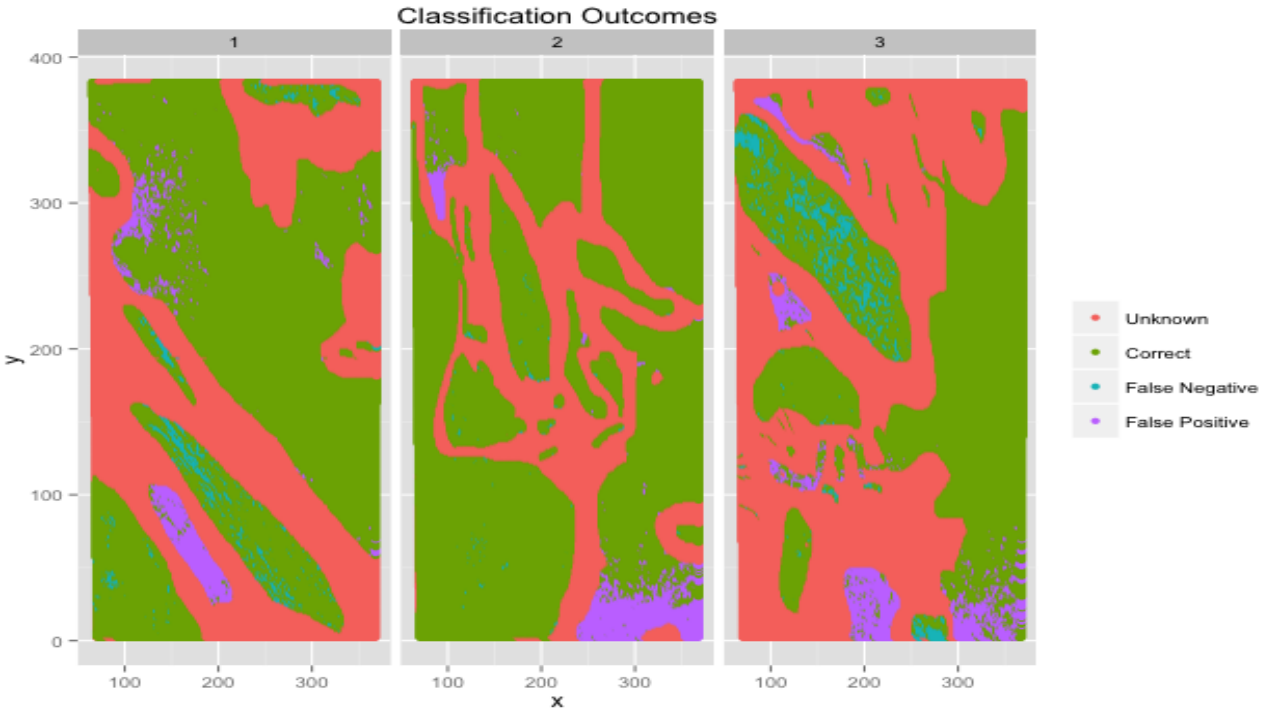

Figure 16: Classification results from logit with respect to the expert labels.

We now discuss the trends in misclassification. As depicted in the above figure, we have many more false positives than false negatives with large regions sometimes completely misclassified. These regions are often situated on boundaries of labelled and unlabelled points. Calculation shows the false negative rate to be 7.5% and the false positive rate to be 11.7%.

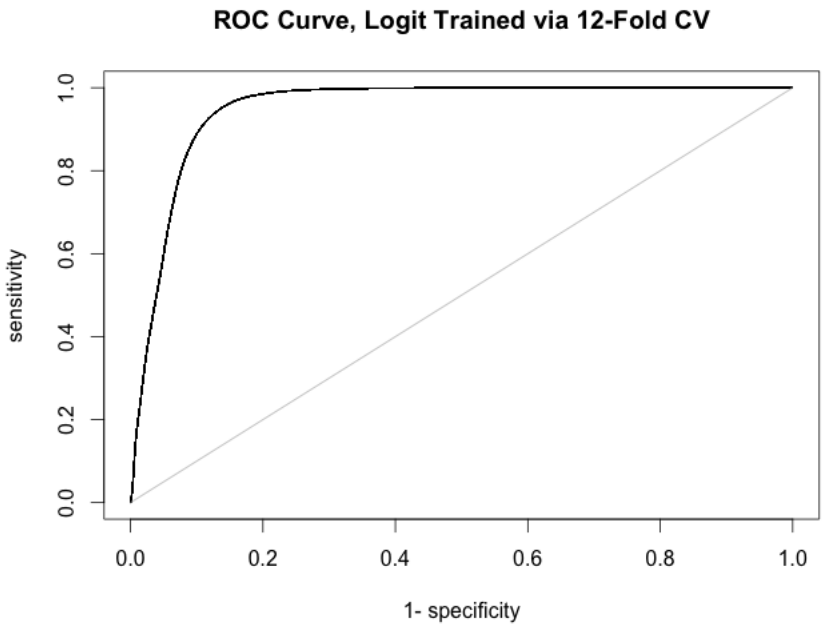

Figure 17: ROC curve for our logit model. AUC is .95.

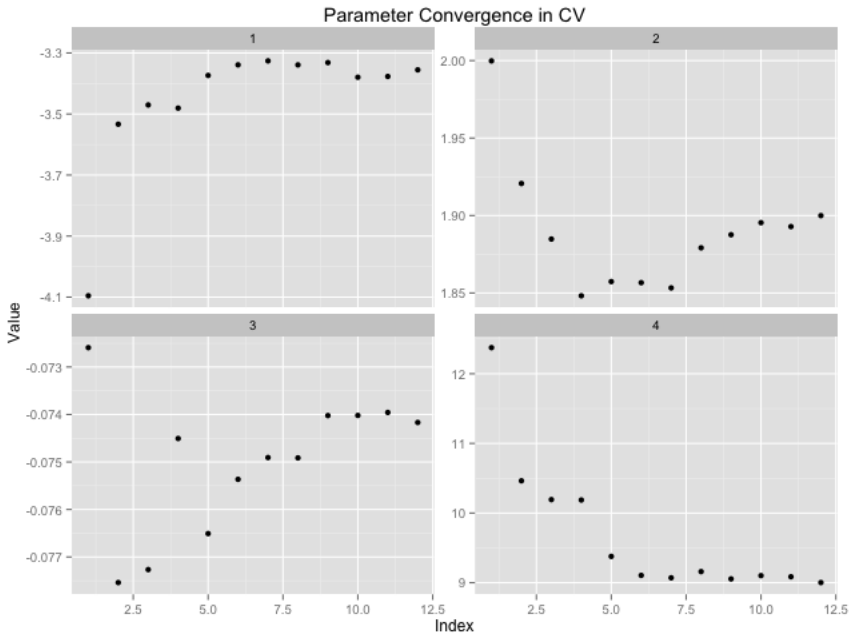

Figure 18: Coefficient values through iterations of 12-fold CV.

3.3 Random Forest

For random forest, as in all the other classifiers, we divided the three images into equal sized quadrants (2X2) rectangles in order to do 12 fold validation on the dataset. That is, for each iteration of the validation, we dropped one of the quadrants as a test set, and trained on the remaining 11 quadrants. Keeping the test segments as disjoint chunks from the test set ensured that our models were picking up on 'higher' level structure of the dataset, and not the continuous variation of neighbouring pixels. As such, we also expect the performance of the model on these test sets to be a much better predicator of how our model will perform on new images than if we randomly subsampled the validation folds. Indeed, after doing random subsampling, we noticed that the AUC was at a high 0.999 for all cross validations, whereas by cross validating on the isolated quadrants, our AUC curves had much higher variance, as seen below:

	AUC
1st fold	0.996600222048787
2st fold	0.960408561886229
3st fold	0.629930590380754
4st fold	0.995687025393392
5st fold	0.999193970074872
6st fold	0.973449221681138
8st fold	0.945314282554696
9st fold	0.996766914151693
10st fold	0.594564820737272
11st fold	0.788939754299337
12st fold	0.946931831284243

S S

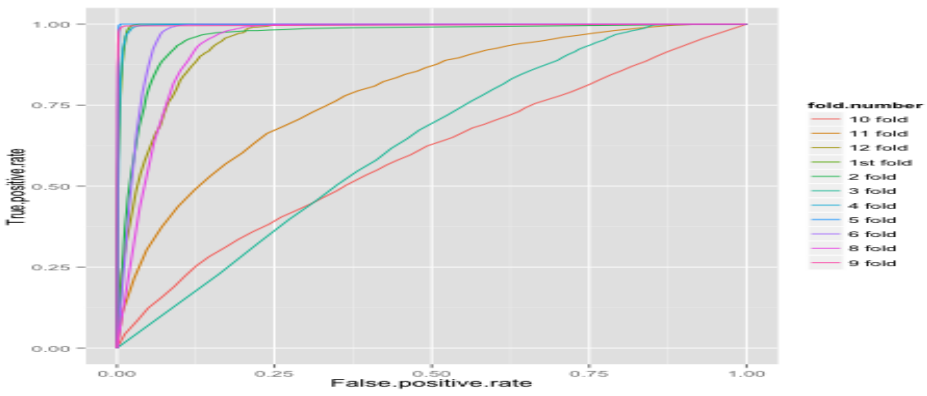

Figure 19: ROC across all 12 folds of quadrants

We also trained on each image and tested on the remaining two.

	AUC
Image 1	0.922460725112444
Image 2	0.903695033714336
Image 3	0.891518876193915

SS

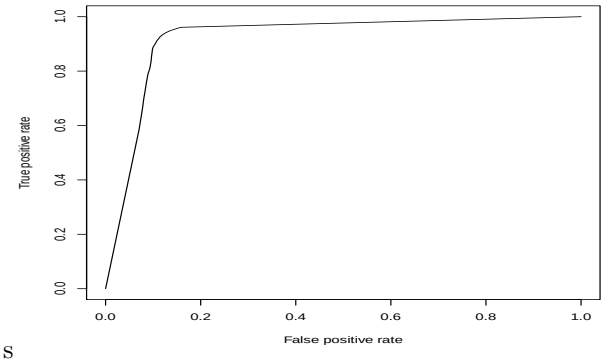

S

Figure 20: Convergence of ROC training on increasing number of quadrants in shuffled order

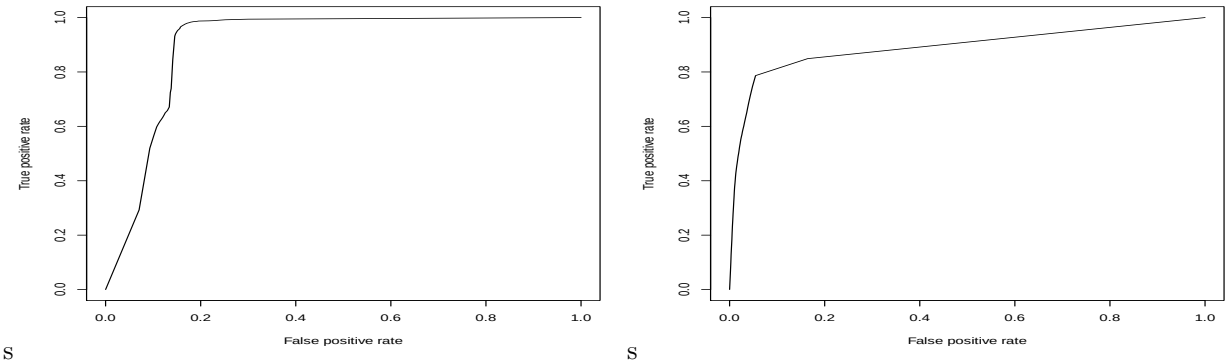

S S

Figure 21: Convergence of ROC training on increasing number of quadrants in shuffled order

To test convergence, one of the things we did was increase the training set from including 1 quadrant, to including 2 quadrants, up to including 11 quadrants (using the complement as the test set). For each of the 3 aforementioned classes of training, we trained on a range of forest sizes, from 2 trees to 50. It was interesting to note that the continuity of increasing the training set by neighbouring quadrants displayed much less convergence than by increasing the training quadrant set in a randomly subsampled way. The following three plots make this clear. In the first case....

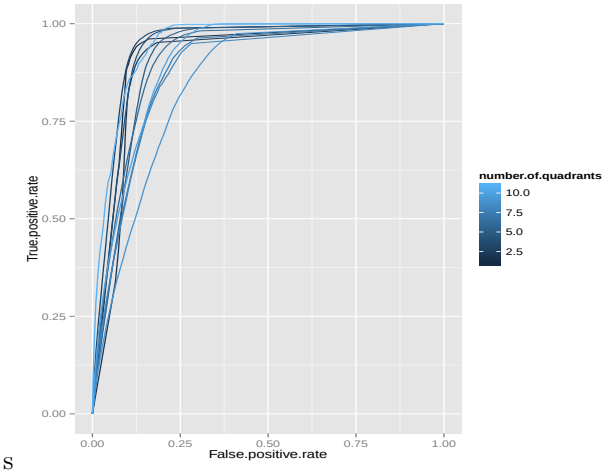

S

Figure 22: Convergence of ROC training on increasing number of quadrants

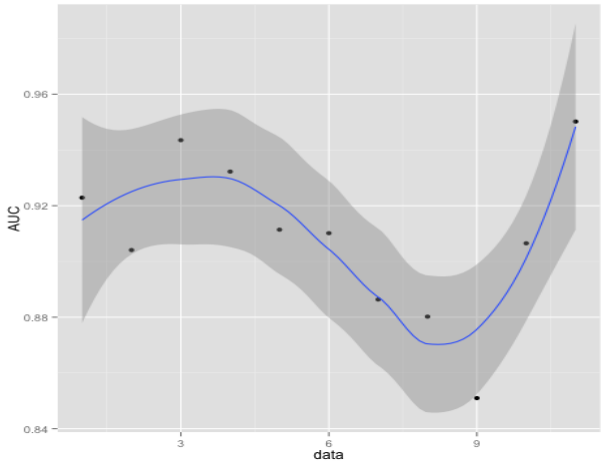

S

Figure 23: Smoothed convergence of AUC for growing training set 50 trees and 3 features

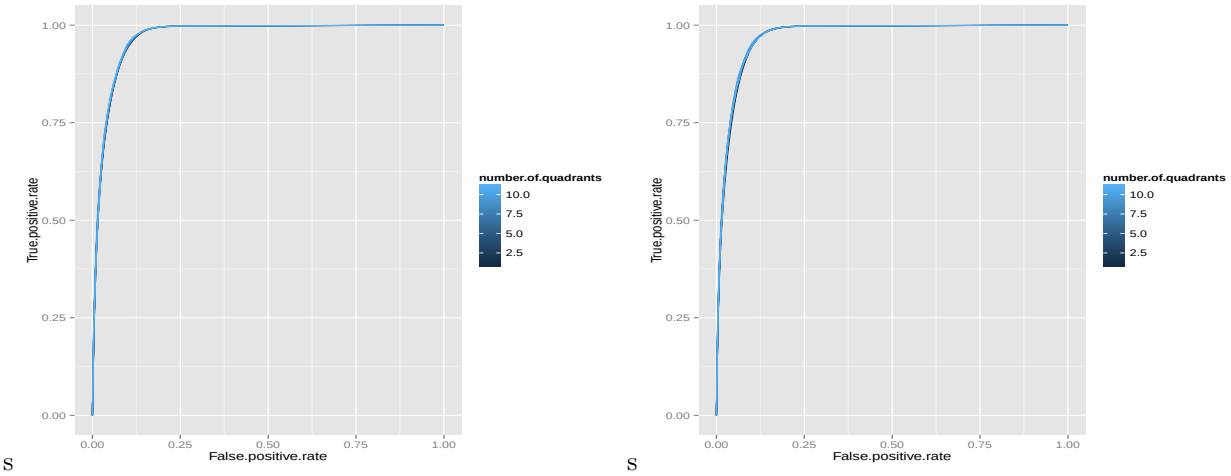

Figure 24: Convergence of ROC training on increasing number of quadrants in shuffled order

To gather a quantitative measurement of the importance of each feature, we first ran random forest using all the features and looked at the GIni importance measure. This is calculated by recording the difference between the Gini measure of a random forest's predictions on a fold and the Gini measure with a particular feature's values randomly shuffled. The intuition is that if a feature were crucial to the forest's trees, than randomly shuffling that feature will drastically decrease it's Gini measure. Sure enough, NDAI, SD and CORR consistently ranked as the clear top three in all cross validations.

Where was the model performing poorly?

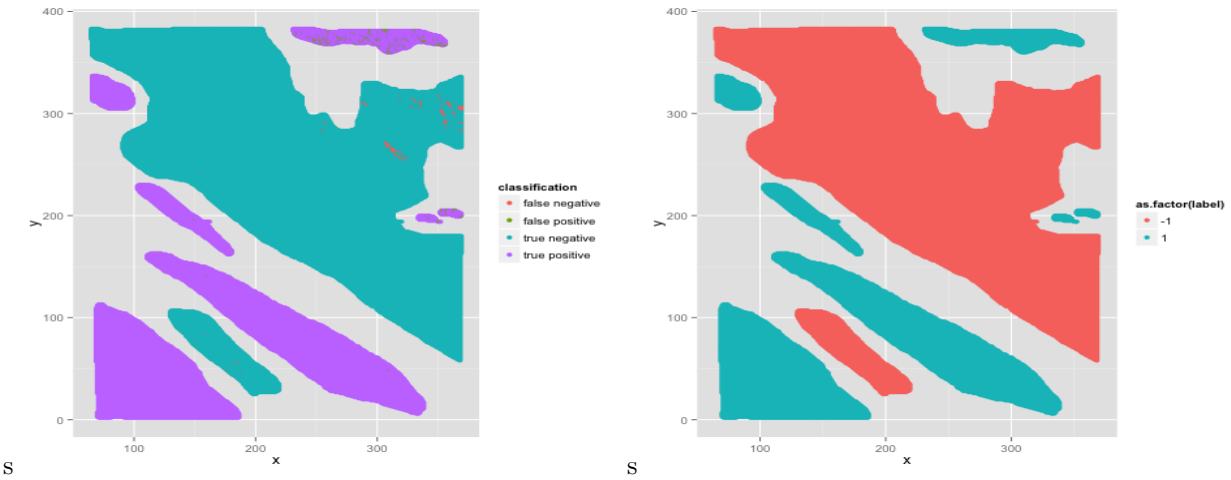

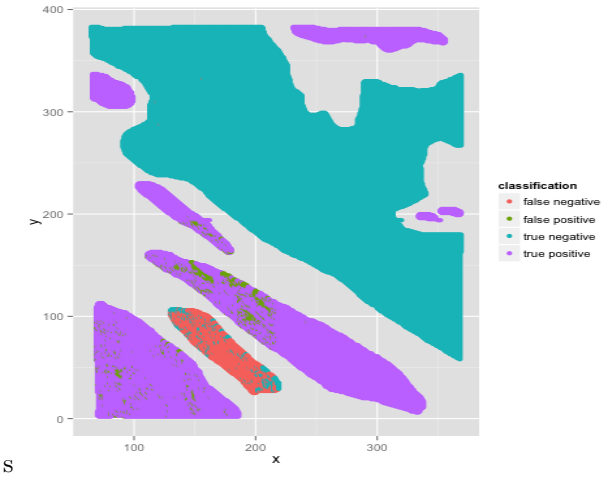
400
300
200
100
0
y
100
200
300
x
classification
false negative
false positive
true negative
true positive

S


400
300
200
100
0
y
100
200
300
x
as.factor(label)
-1
1

S

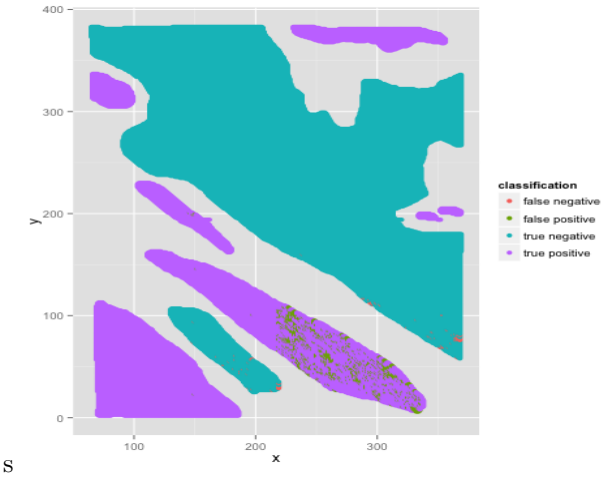
400
300
200
100
0
y
100
200
300
x
classification
false negative
false positive
true negative
true positive

S

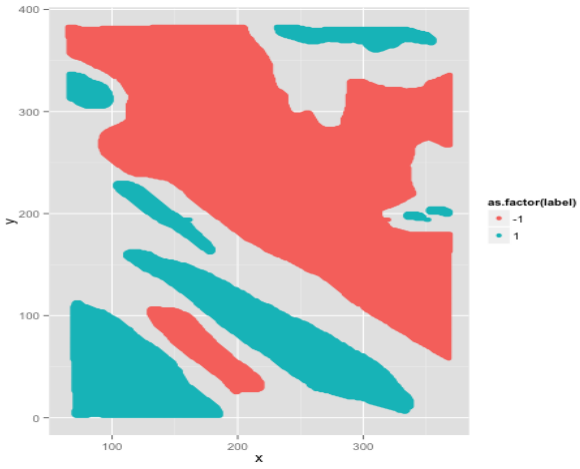
400
300
200
100
0
y
100
200
300
x
as.factor(label)
-1
1

S

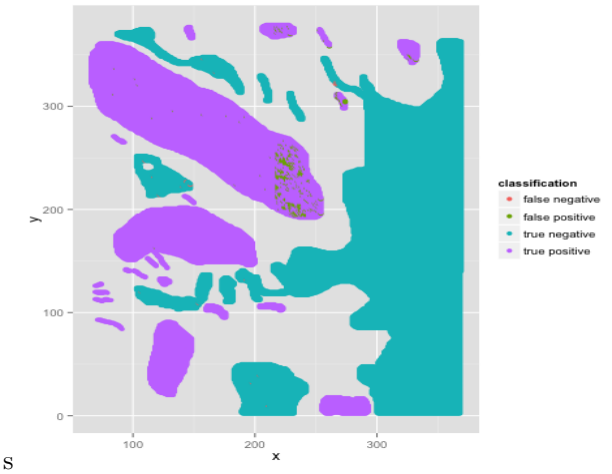
300
200
100
0
y
100
200
300
x
classification
false negative
false positive
true negative
true positive

S

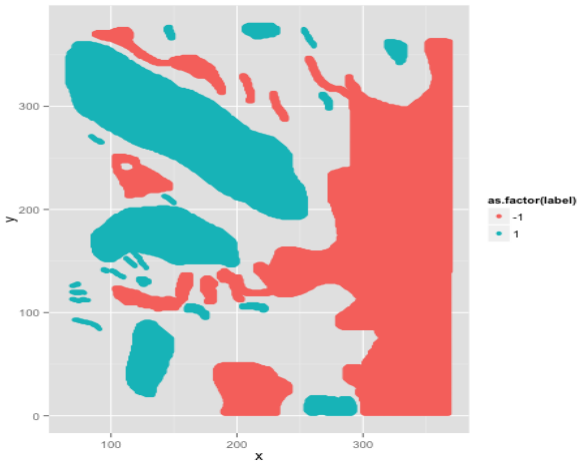
300
200
100
0
y
100
200
300
x
as.factor(label)
-1
1

S

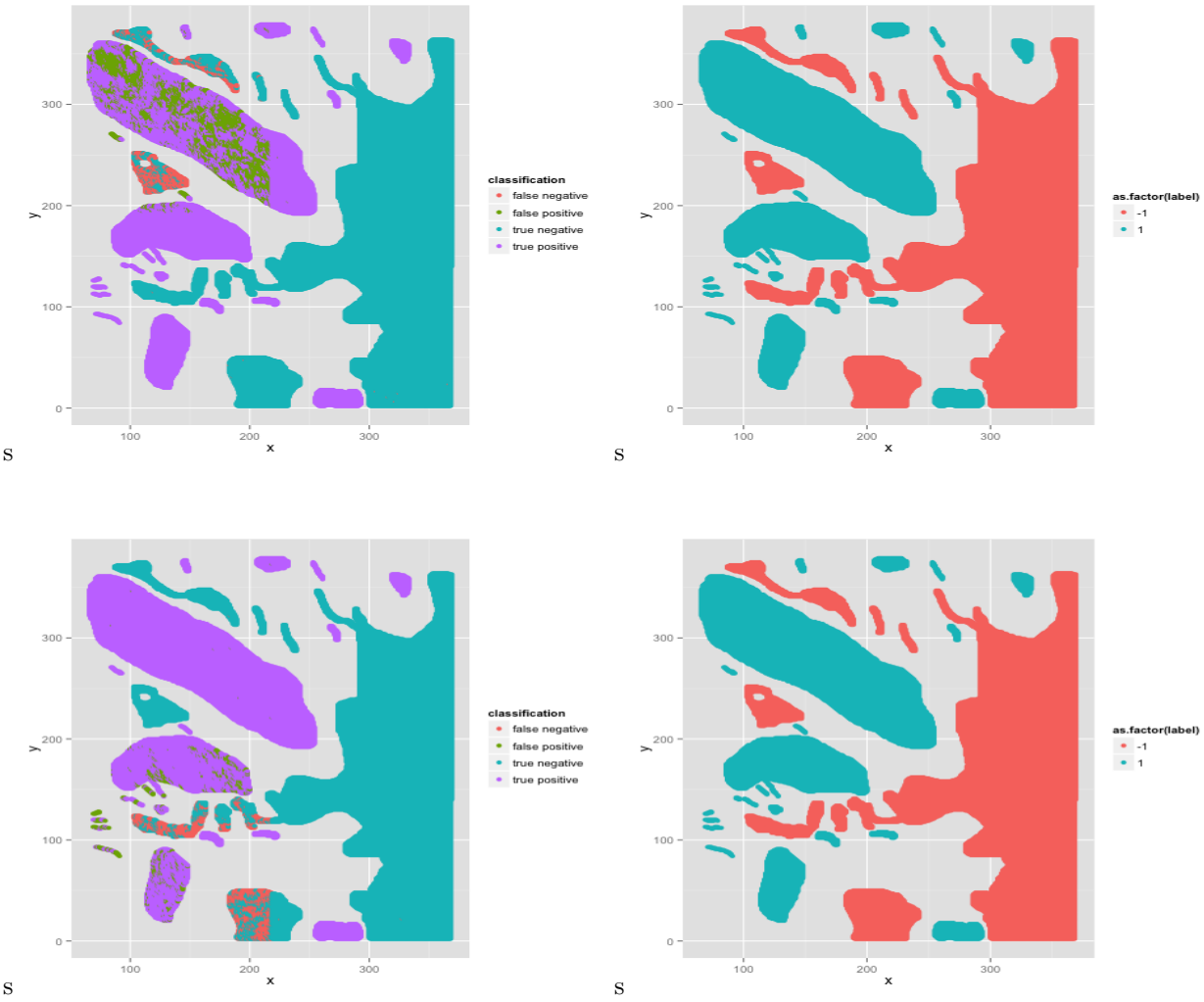

4 Reproducibility

How we organized out code and github repo

	mean	variance	sd
NDAI	31851.137865015	5541519.63141267	2354.04325181435
SD	15181.3036164789	7250037.34195744	2692.58933778574
CORR	16696.8895555848	15065266.3880018	3881.40005513498
DF	5153.57742916125	715182.664503553	845.684731151954
CF	3725.98512846366	238611.088513114	488.478339860749
BF	4741.67090014784	908691.31228918	953.253015882551
AF	6307.45653651382	1489619.01113017	1220.49949247436
AN	7656.24468437671	5730133.08077185	2393.76963820077

Figure 25: Mean Gini Importance Measure across 12 folds

References

[1] Ben-Hur, A., Elisseeff, A., Guyon, I.: A stability based method for discovering structure in clustered data. In: Pacific Symposium on Biocomputing, pp. 617.